Switchable Plasmonic-Dielectric Resonators with Metal-Insulator Transitions

Nikita A. Butakov[1], Ilya Valmianski[2], Tomer Lewi[1], Christian Urban[2], Zhensong Ren[3], Alexander A. Mikhailovsky[4], Stephen D. Wilson[5], Ivan K. Schuller[2], Jon A. Schuller[1]
[1]*University of California, Santa Barbara, Department of Electrical & Computer Engineering*
[2]*University of California, San Diego, Department of Physics and Center for Advanced Nanoscience*
[3] *Boston College, Physics Department*
[4]*University of California, Santa Barbara, Department of Chemistry and Biochemistry*
[5]*University of California, Santa Barbara, Materials Department*
e-mail address: schuller@ece.ucsb.edu

Abstract

Nanophotonic resonators offer the ability to design nano-scale optical elements and engineered materials with unconventional properties. Dielectric-based resonators intrinsically support a complete multipolar resonant response with low absorption, while metallic resonators provide extreme light-confinement and enhanced photon-electron interactions. Here, we construct resonators out of a prototypical metal-insulator transition material, Vanadium Dioxide (VO_2), and demonstrate switching between dielectric and plasmonic resonances. We first characterize the temperature-dependent infrared optical constants of VO_2 single-crystals and thin-films. We then fabricate VO_2 wire arrays and disk arrays. We show that wire resonators support dielectric resonances at low temperatures, a damped scattering response at intermediate temperatures, and plasmonic resonances at high temperatures. In disk resonators, however, upon heating there is a pronounced enhancement of scattering at intermediate temperatures, and a substantial narrowing of the phase transition. These findings may lead to the design of novel nanophotonic devices that incorporate thermally switchable plasmonic-dielectric behavior.

Keywords: tunable metasurfaces, metal-insulator transition, phase change materials, vanadium dioxide

Nanophotonic resonators have made an enormous impact on nanoscale science and engineering. Metallic resonators that support plasmonic excitations have enabled extreme concentration of light[1], near-field imaging microscopes that surpass the diffraction limit[2], plasmon-driven catalytic processes[3,4], antennas with localized heat generation[5], and metamaterials that support hyperbolic optical response[6]. The more recent development of dielectric Mie-type resonators, which intrinsically support a multipolar response with both electric and magnetic modes, have further expanded the available parameter space for nanophotonic design[7-9]. Dielectric resonators are used for a wide range of functionalities including evanescent wave skin-depth engineering[10], amplification of non-linear processes[11], and local enhancement of magnetic fields[12,13]. Furthermore, dielectric metasurfaces offer the potential ability to replace large traditional optics with high efficiency, compact, nano-scale optical elements. By spatially varying the geometry across a surface, flat optical components were recently demonstrated, including lenses[14,15,16], blazed gratings[17,18,19], vortex plates[20,21], and beam-shaping metasurfaces[22,23].

There is substantial interest in developing nanophotonic devices with dynamically reconfigurable properties[24]. To satisfy this need, various physical mechanisms have been pursued, including electrical carrier injection/depletion of semiconductors[25,26], amorphous-crystalline phase changes in dielectrics[27,28,29], nano-mechanical tuning of resonators[30], ultrafast pumping[31,32], thermo-optic tuning[33], voltage gating of graphene[34], and metal-insulator transitions (MIT) in strongly correlated materials[35,36,37,38,39,40]. In this work, we demonstrate active index-tunable resonators comprising the prototypical strongly correlated material, vanadium dioxide (VO_2). Exploiting a temperature-driven MIT, we demonstrate large shifts in the multipolar resonant behavior as resonators switch between plasmonic and dielectric regimes. In contrast to previous work on VO_2 optical elements[41,42,43,44], these metamaterial resonators support switching between dielectric Mie resonances and plasmonic resonances. We grow single crystals and thin films of VO_2 and characterize the infrared optical permittivity across the MIT. We then fabricate and experimentally characterize VO_2 wire arrays and disk arrays. We find that VO_2 wire arrays exhibit a polarization-dependent dielectric resonance at low temperatures, a suppressed scattering response at intermediate temperatures, and a plasmonic resonance at high temperatures. The VO_2 disk arrays on the other hand, exhibit enhanced scattering at intermediate temperatures and a narrowed metal-insulator transition. This proof-of-concept

paves the way towards constructing thermally tunable metasurfaces that integrate switchable plasmonic-dielectric behavior.

Tunable Optical Constants

Strongly correlated materials are substances in which strong electron-electron interactions lead to emergent properties such as superconductivity, colossal magnetoresistance, and Mott-Hubbard metal-insulator phase transitions[45]. When heat, voltage, or magnetic fields are applied to such materials the optical constants may also undergo dramatic shifts. In Fig. 1a, we plot the reflectivity of a VO_2 single crystal in its insulating and metallic phases, and, in Fig. 1b, we plot the fitted optical permittivity. The insulating phase is characterized by a flat reflection spectrum with R≈0.25, corresponding to a permittivity ε≈9 (refractive index n≈3), slightly lower than that of Silicon (n≈3.4). The metallic phase is characterized by a dispersive reflection spectrum typical of low conductivity metals, which corresponds to a Drude permittivity model with plasma frequency ω_p=413 THz and scattering rate γ=74 THz.

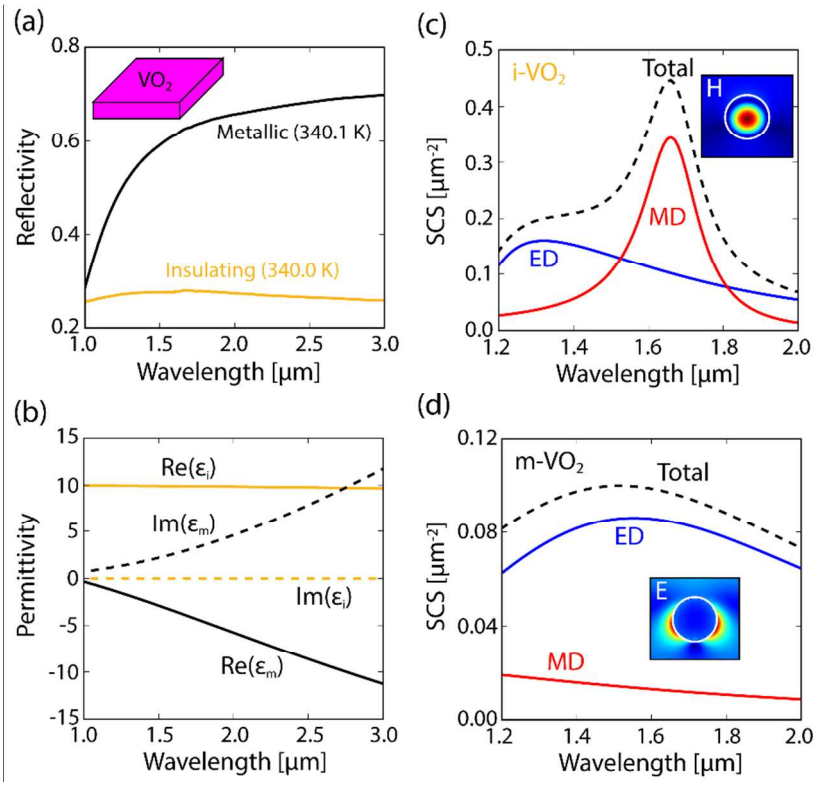

Figure 1 – **Reflectivity of VO_2 Single Crystals. (a)** Near-infrared reflectivity of a VO_2 single crystal in its low-temperature insulating phase (orange curve) and high-temperature metallic phase (black curve). **(b)** Real (solid curve) and imaginary (dashed curve) components of the fitted VO_2 optical permittivity in the insulating phase (orange curve) and metallic phase (black curve). Scattering-cross-section of a **(c)** insulating, and **(d)** metallic VO_2 sphere in air, with diameter d=500 nm, calculated with Mie theory. Insets corresponds to simulated local (c) magnetic, and (d) electric, field profile at the fundamental resonance. Crystal growth, optical characterization, Mie Theory calculation, and simulation details are included in the Supporting Information.

The contrast in reflectivity and permittivity is most pronounced at wavelengths beyond 1.5 μm. We plot the scattering-cross-section of a 500 nm VO_2 sphere, calculated with Mie theory, in the insulating (Fig. 1c) and the metallic (Fig. 1d) phases. In both phases, a fundamental scattering resonance occurs near 1.65 μm. However, this resonance is primarily a magnetic-dipole mode in the insulating phase and an electric-dipole mode in the metallic phase. The electric and magnetic profiles are shown in insets of Fig. 1c and 1d. Such resonators can therefore be used as the basis for optical antennas that switch from magnetic to electric resonant behavior. In the Supporting

Information we experimentally investigate the behavior of individual Vanadium Oxide spherical resonators, fabricated with femtosecond laser ablation.

In free-standing single crystals the metal-insulator transition is sharp and characterized by phase boundary propagation from few nucleation sites[46]. In thin-films, a more common medium for nanophotonic resonators, defects generate many nucleation sites, leading to a broadened percolative transition[47]. As the insulating film is heated, nanoscale metallic inclusions nucleate and percolate into a fully metallic film[48]. Optically, the film acts as an effective medium, providing continuous access to intermediate states with optical constants averaged between the insulating and the metallic clusters. In Fig. 2a, we plot the infrared reflectivity of a 100 nm thick VO_2 film on a sapphire substrate at various temperatures. In the insulating phase, the film exhibits a Fabry-Perot resonance near $\lambda=4nt=1.2$ μm, where n is the refractive index and t is the film thickness. Note that this is a reflection *maximum* due to the larger index of refraction in VO_2 in comparison to the sapphire substrate. As the temperature increases the feature smears out due to increased losses, culminating in a near flat response at an intermediate temperature of 341K. Although intermediate values of Re[ε] are accessed at intermediate temperatures (Fig. 2b), the sharp rise in losses (Fig. 2c) precludes any clear shifting of the Fabry-Perot resonance wavelength. There is also a local minimum in Re[ε] due to the presence of an absorption resonance. This local minimum is not present in single-crystals and might be due to defects in the thin film. At higher temperatures, metallic behavior ultimately sets in.

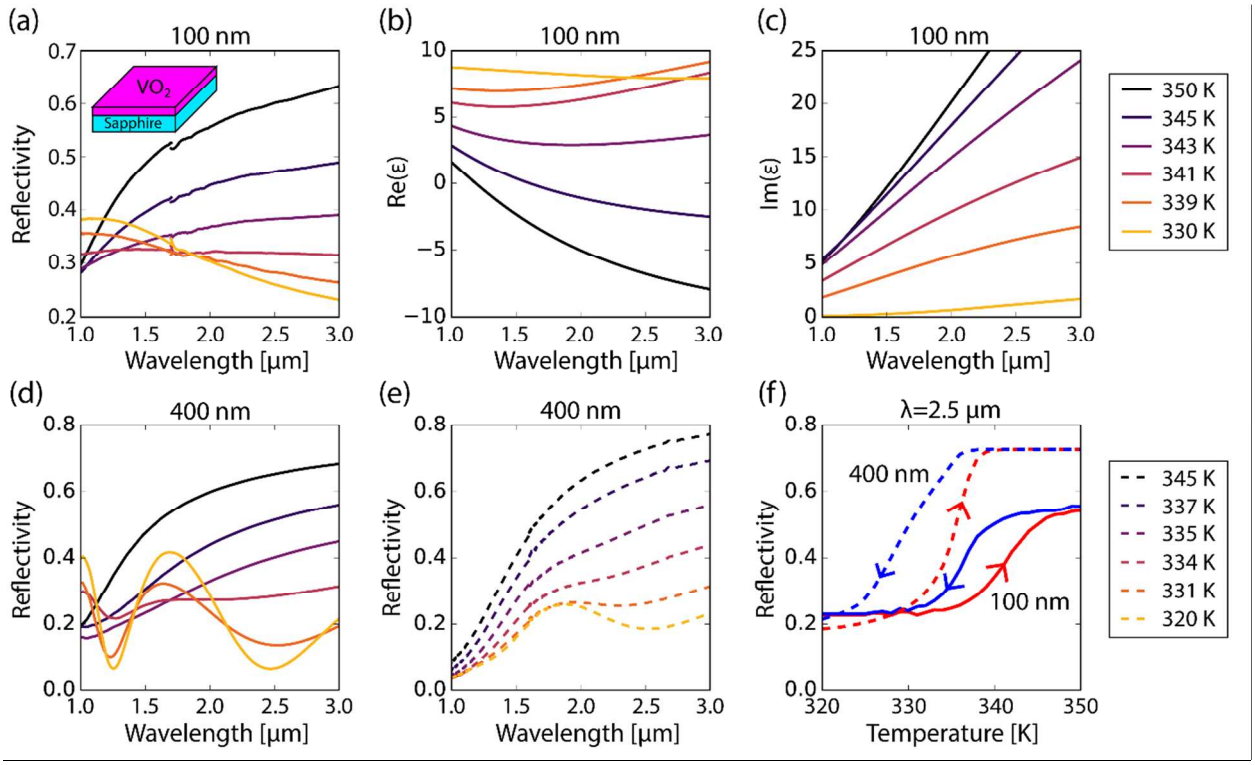

Figure 2 – **VO_2 Thin-Film Reflectivity and Optical Constants (a)** The measured FTIR reflectivity of a 100 nm VO_2 film on a sapphire substrate. The **(b)** real, and **(c)** imaginary components of the optical permittivity, as determined by a spectral fit to the measured reflectivity. Experimental and fitting details are provided in the Supporting Information. **(d)** The simulated reflectivity of a 400 nm thick VO_2 film, based on the 100 nm optical constants. **(e)** The measured reflectivity of a 400 nm thick VO_2 film. **(f)** The optical hysteresis of the 100 nm film (solid line) and 400 nm film (dashed line) at a wavelength $\lambda=2.5$ μm. Sample fabrication, measurement details, and mid-infrared spectra are included in the Supporting Information.

As the film is heated through the MIT, the initially positive permittivity, $\varepsilon\approx9$, continuously decreases, passes through zero, and becomes negative, corresponding to the metallic phase. When fully metallic, the Drude fit has a plasma frequency $\omega_p=981$ THz and scattering rate $\gamma=205$ THz. The larger scattering rate, as compared to single

crystals, may be attributed the larger number of defects in the films in the form of grain boundaries, crystallographic defects, and surface roughness. This full span of permittivity, corresponding to capacitive (dielectric), inductive (metallic), and resistive (intermediate) optical behavior, signifies that VO_2 may be well-suited for the design of reconfigurable devices based on optical circuit concepts[49].

In order to support high-quality dielectric-type resonances in the infrared spectral range, where permittivity contrast is large, the VO_2 film must be relatively thick. In Fig. 2d, we plot the simulated reflectivity of a 400 nm thick VO_2 film deposited on a sapphire substrate based on the extracted optical constants of the 100 nm film. In the fully insulating low-temperature phase (yellow), we observe a series of higher-order Fabry-Perot peaks corresponding to $\lambda = 4nt/3 \approx 1.6\mu m$ and $\lambda = 4nt/5 \approx 1.0\mu m$. In the high-temperature metallic phase (black), the simulated reflection again exhibits a typical Drude reflectivity profile. In Fig. 2e, we plot the experimentally measured reflectivity of a 400 nm thick VO_2 film on a sapphire substrate. The observed peak near 1.6 μm in the insulating phase, similar to the one seen in simulation, reveals a Fabry-Perot mode corresponding to a film refractive index of 3. A subsequent Fabry-Perot reflection minimum is observed near 2.5 μm in both simulation and experiment. The lack of an experimentally observed higher-order mode at 1 μm, however, suggests that there are significant differences between the optical constants of thin and thick films. A good fitting of the thick film optical constants could not be obtained due to increased surface roughness which suppresses specular reflection at shorter wavelengths.. Islands of non-stoichiometric VO_x, and strain-relaxation effects[50], may also contribute to differences between simulated (based on thin-film constants) and measured results at short wavelengths. Compared to the 100 nm film, the thick-film MIT temperature is reduced by 5-7 K (Fig 2f) which may be attributed to oxygen deficiency[51]. Additionally, the change in sheet resistance across the MIT is three orders of magnitude lower than the 100nm films (Fig. S4), indicating a clear difference in film quality.

In subsequent simulations, we use the fitted optical constants of the 100 nm films to understand the behavior of resonators that undergo metal-insulator phase transitions. This data is publicly available in our supporting information. It is important to note that between films there may be variations in the reflectivity and, hence, optical constants due to differences in stoichiometry, substrate-induced strain, film thickness, grain size, and surface roughness.

Wire Arrays

Semiconductor wires, when confined to sub-wavelength scales, support a series of multipolar Mie resonances[52,53,54]. Such structures are of interest for improved solar absorbers[55,56], photodetectors[57], and color filters[58]. Here we examine the behavior of a VO_2 wire array as it undergoes a metal-insulator transition. In Fig. 3a, we plot the simulated reflectivity in the insulating phase (orange curve) and metallic phase (black curve). The incident light is transverse-electric (TE) polarized with electric-field perpendicular to the wire orientation. The fundamental dielectric resonance at $\lambda \approx 1.25$ μm has a strong magnetic-field inside the wire (inset of Fig. 3a) and is a magnetic-dipole-like mode. The metallic resonance at $\lambda \approx 1.6$ μm on the other hand, is an electric-dipole-like mode. Similar to spheres (Fig. 1c and d), wire resonators support both dielectric- and metallic-type resonances in the same wavelength regime, but with different field symmetries. In the experimentally measured reflection spectrum (Fig. 3b) we observe similar reflection profiles and switching between magnetic and electric dipole resonances. The experimentally measured reflection is reduced however, due to surface roughness. In Fig. 3c we plot the simulated reflection spectra, including intermediate temperatures. At intermediate temperatures (dashed line near 340K), there is a broadband suppression in scattering. This effect, similar to that observed in a previous work[59], may be attributed to the relatively large loss tangent ($\mathrm{Im}[\varepsilon]/\mathrm{Re}[\varepsilon]$) when the VO_2 passes through its epsilon-near-zero condition, and may be used to construct efficient amplitude modulators. Experimentally, we observe similar behavior in Fig. 3d although decreased in amplitude, shifted to lower wavelength, and increased in the transition temperature. Similar behavior is observed under transverse-magnetic polarization (supporting information).

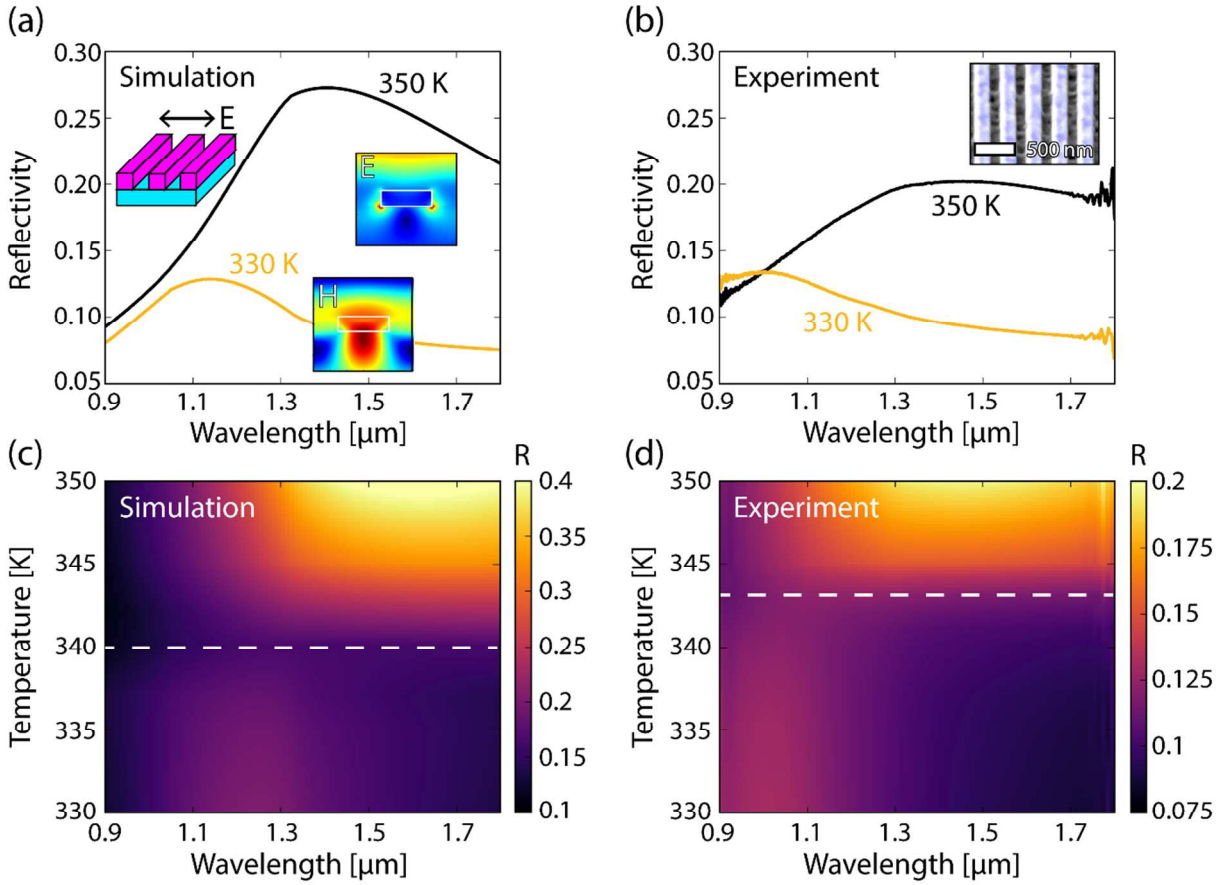

Figure 3 – **TE-Polarized VO_2 Wire Array Reflectivity. (a)** Simulated reflectivity of a VO_2 wire array, on sapphire, in the insulating and metallic phases, under TE-polarized illumination based on optical constants found for a 100 nm VO_2 film. Insets corresponding to the magnetic-field profiles at the insulating resonance, and electric-field profiles at the metallic resonance. **(b)** Experimentally measured reflectivity of the corresponding VO_2 wire array, in the insulating and metallic phases. Inset is an SEM of the fabricated structure. **(c)** Simulated, and **(d)** experimentally measured, reflectivity of the array, including intermediate temperatures. Note that the color scale in (d) is different relative to (c) to increase clarity. Wires are rectangular with width w=280 nm, height h=100 nm, and pitch a=500 nm. Simulation and experimental details are included in the Supporting Information.

Disk Arrays

VO_2 disk resonators are expected to exhibit more pronounced resonant features due to increased electromagnetic confinement. In Fig. 4a, we plot the simulated reflection spectra of a VO_2 disk array above and below the transition temperature. In the fully insulating phase (orange curve), the reflectivity peaks at $\lambda \approx 1.5$ μm, corresponding to the magnetic dipole resonance. As the array is heated across the transition, the resonance red-shifts and increases in amplitude, becoming a plasmonic electric dipole mode near $\lambda \approx 1.7$ μm (black curve). In Fig. 4b, we plot the complete simulated temperature-wavelength reflectivity dependence. Similar to the wire array, there is suppressed scattering at intermediate temperatures. In Fig. 4c, we plot the experimentally-measured reflection of a VO_2 disk array below and above the MIT. In the low-temperature insulating phase (orange curve) the measured response has a reflection peak at $\lambda \approx 1.5$ μm, in agreement with the simulated response. Upon heating, the array transitions from fully insulating behavior at 334 K to fully metallic behavior at 340 K, a substantially narrower transition that one found in the wire arrays or thin films. In the metallic phase (black curve), the measured response has a reflection peak at $\lambda \approx 1.3$ μm, slightly blue-shifted and with overall lower reflectivity value relative to the

simulation, which may be attributed to surface roughness and potentially direct contact between resonators. However, examining the experimentally-measured reflection, upon heating, (Fig. 4d) at intermediate temperatures there is a pronounced *enhancement* of reflection. Such behavior could be expected of a dielectric resonator with an increased refractive index, or a plasmonic resonator with an increased plasma frequency or reduced Drude scattering rate. It may also perhaps be attributable to strong-correlation effects in the vicinity of phase transition, which have been observed by others. Another potential explanation is the "critical opalescence" effect observed in inhomogeneous mixtures. Similar behavior was recently observed for VO_2 particle arrays in the visible spectrum[60]. The effect was attributed to the random nature of the phase transition, in which individual particles randomly become metallic at different temperatures. This behavior is only present upon the heating portion of the hysteresis loop. Upon cooling (Fig. 4e) there is a suppression of reflection at intermediate temperatures, similar to the wire arrays. Such asymmetries may be attributable to the differing nucleation mechanisms upon heating and cooling[61]. Further studies are necessary to conclusively understand the origin of this enhanced scattering.

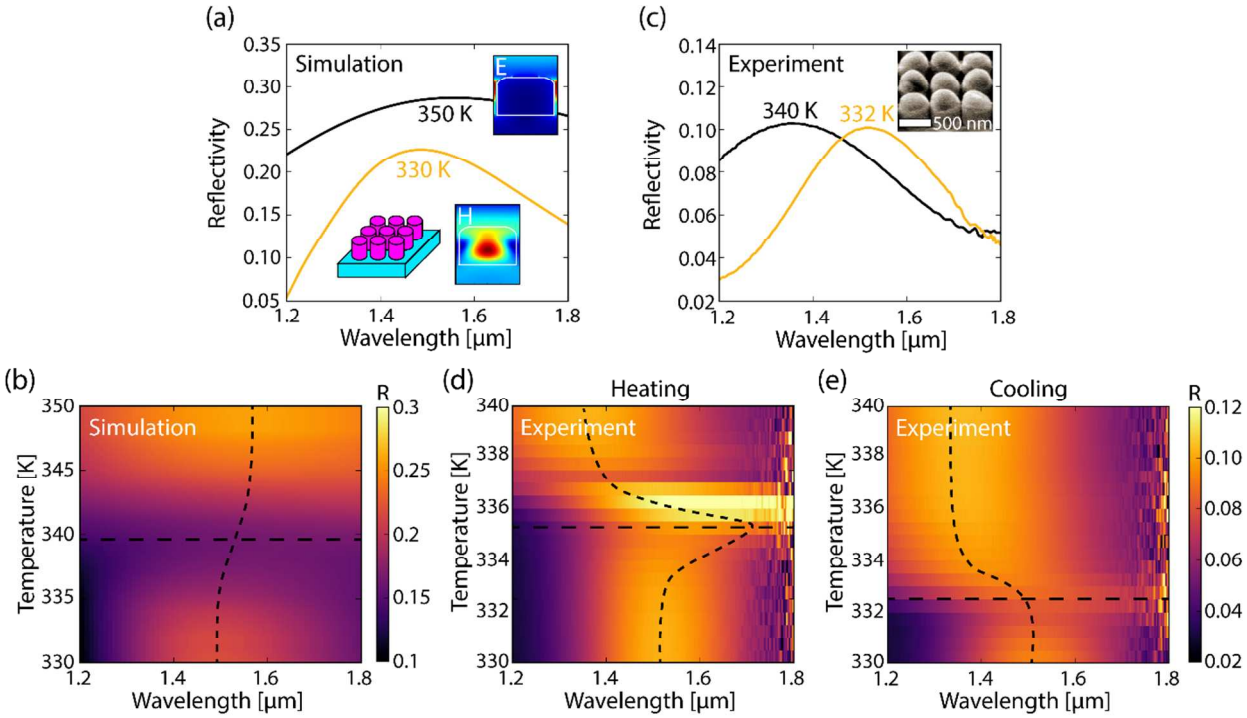

Figure 4 –**VO_2 Disk Array Reflectivity**. **(a)** Simulated reflectivity of a VO_2 disk array. Disk resonators have a height h=500 nm, diameter d=480 nm, and pitch a=500 nm based on optical constants from a 100 nm film. Insets correspond to local field distributions at the resonant peaks. **(b)** Simulated reflection as a function of temperature and wavelength. Vertical dashed curve tracks the reflectivity peak, horizontal dashed line represents the transition temperature **(c)** Experimentally measured reflectivity of VO_2 disk array (with approximate height h=400 nm, diameter d=480 nm, and pitch a=500) above and below transition. Inset is an SEM of the fabricated structure. **(d)** Experimental reflection data, upon heating, including intermediate temperatures. **(e)** Experimental reflection data, upon cooling, including intermediate temperatures. Vertical dashed curve tracks the reflectivity peak, horizontal dashed line represents the transition temperature. Note that the temperature span in (d,e) is different than (c). Simulation and experimental details are included in the Supporting Information.

Future work on controlling the MIT of VO_2 nanophotonic devices, such as strain engineering[62,63], electrically controllable resonators[64,65] and spatially-modulated optical pumping[66], may enable the development of high-performance reconfigurable metasurfaces. In previous works, tuning of statically-doped and photo-excited semiconductor resonators was demonstrated, in which dense electron-hole charge densities led to plasmonic optical behavior[67,68,69,70]. VO_2 resonators, in contrast, display dynamic switching between dielectric and plasmonic behavior

over extremely narrow temperature spans, making them particularly intriguing for energy efficient applications. Finally, although here we demonstrated the basic behavior with VO_2, similar phenomena hold for other correlated materials such as V_2O_3[71,72], $SmNiO_3$[73], and $NdNiO_3$[74].

Conclusion

We demonstrate that the metal-insulator transition of a prototypical strongly correlated material, VO_2, may be used to construct thermally tunable structures that exhibit a dual plasmonic-dielectric resonant response. Through FTIR reflectivity measurements we extract the optical permittivity of VO_2 single crystals and thin-films above and below the MIT, allowing access to the full span of positive, zero, and negative optical permittivity. In fabricated arrays of VO_2 wires, we experimentally demonstrate dielectric resonances at low temperatures, a damped scattering response at intermediate temperatures, and a plasmonic resonance at high temperatures. Similar behavior occurs in disk resonators; however, increased confinement leads to several unusual effects. There is a substantial narrowing of the transition temperature width, such that switching occurs over less than 4 K. And there is a pronounced enhancement, rather than suppression, of scattering at intermediate temperatures. These novel, dynamically tunable optical behaviors of VO_2 resonators demonstrate that materials with metal-insulator phase transitions hold great promise for future meta-devices.

Supporting Information

Included in the Supporting Information are the experimental and simulation details, experimental data of wire arrays in TM-polarization, measurements of Vanadium oxide spheres, measurements of randomly arranged disk resonators, a Mathematica notebook containing the code used for Mie Theory calculations, and the extracted optical constants of the 100nm VO_2 thin-film.

References

1 Schuller, J. A., Barnard, E.S., Cai, W., Jun, Y.C., White, J.S., and Brongersma, M.L.. Plasmonics for extreme light concentration and manipulation. Nat. Mater., 2010, 9, 193-204 .

2 Betzig, E. and Trautman, J. K. Near-field optics: microscopy, spectroscopy, and surface modification beyond the diffraction limit. Science, 1992, 257, 189-195.

3 Zhang, X., Chen, Y.L., Liu, R.S. and Tsai, D.P. Plasmonic photocatalysis. Rep. Prog. Phys. , 2013, 76, 046401.

4 Christopher, P., Xin, H. and Linic, S. Visible-light-enhanced catalytic oxidation reactions on plasmonic silver nanostructures. Nat. Chem. , 2011, 3, 467-472.

5 Hirsch, L.R., Stafford, R.J., Bankson, J.A., Sershen, S.R., Rivera, B., Price, R.E., Hazie, J.D., Halas, N.J., and West, J.L. Nanoshell-mediated near-infrared thermal therapy of tumors under magnetic resonance guidance. Proc. Natl. Acad. Sci. , 2003, 100, 13549-13554.

6 Poddubny, A., Iorsh, I., Belov, P. and Kivshar, Y. Hyperbolic metamaterials. Nat. Photonics 7, 948-957 (2013).

7 Jahani, S. and Jacob, Z. All-dielectric metamaterials. Nat. Nanotechnol., 2016, 11, 23-36.

8 Das, T., Iyer, P. P., DeCrescent, R. A. and Schuller, J. A. Beam engineering for selective and enhanced coupling to multipolar resonances. Phys. Rev. B, 2015, 92, 241110.

9 Butakov, N. A. & Schuller, J. A. Designing Multipolar Resonances in Dielectric Metamaterials. Sci. Rep., 2016, 6.

10 Jahani, S. and Jacob, Z. Transparent subdiffraction optics: nanoscale light confinement without metal. Optica, 2014, 1, 96-100.

11 Smirnova, D. and Kivshar, Y. S. Multipolar nonlinear nanophotonics. Optica, 2016, 3, 1241-1255.

12 Albella, P. Poyli, M.A., Schmidt, M.K., Maier, S.A., Moreno, F., Saenz, J.J., and Aizpura, J.. Low-loss electric and magnetic field-enhanced spectroscopy with subwavelength silicon dimers. J. Phys. Chem. C, 2013, 117, 13573-13584.

13 Bakker, R. M., Permyakov, D., Yu, Y.F., Markovich, D., Paniagua-Dominguez, R., Gonzaga, L., Samusev, A., Kivshar, Y., Luk-yanchuck, B., and Kuznetsov, A.I. Magnetic and electric hotspots with silicon nanodimers. Nano Lett., 2015, 15, 2137-2142.

14 Arbabi, A., Horie, Y., Ball, A. J., Bagheri, M. & Faraon, A. Subwavelength-thick lenses with high numerical apertures and large efficiency based on high-contrast transmitarrays. Nat. Commun., 2015, 6.

15 Khorasaninejad, M., Chen, W.T., Devlin, R.C., Oh, J., Zhu, A.Y., and Capasso, F. Metalenses at visible wavelengths: Diffraction-limited focusing and subwavelength resolution imaging. Science, 2016, 352, 1190-1194.

16 Lin, D., Fan, P., Hasman, E. & Brongersma, M. L. Dielectric gradient metasurface optical elements. Science, 2014, 345, 298-302.

17 Sell, D., Yang, J., Doshay, S., Zhang, K. & Fan, J. A. Visible light metasurfaces based on single crystal silicon. ACS Photonics, 2016.

18 Khorasaninejad, M. & Capasso, F. Broadband Multifunctional Efficient Meta-Gratings Based on Dielectric Waveguide Phase Shifters. Nano Lett., 2015, 15, 6709-6715.

19 Yu, Y. F., Zhu, A.Y., Paniagua-Dominguez, R., Fu, Y.H., Luk-yanchuk, and Kuznetsov, A.I. High□ transmission dielectric metasurface with 2π phase control at visible wavelengths. Laser Photonics Rev., 2015, 9, 412-418.

20 Zhan, A., Colburn, S., Trivedi, T.K., Dodson, C.M., and Majumdar, A. Low-contrast dielectric metasurface optics. ACS Photonics, 2016, 3, 209-214.

21 Yang, Y., Wang, W., Moitra, P., Kravchenko, I.I., Briggs, D.P., and Valentine, J. Dielectric meta-reflectarray for broadband linear polarization conversion and optical vortex generation. Nano Lett., 2014, 14, 1394-1399.

22 Desiatov, B., Mazurski, N., Fainman, Y. and Levy, U. Polarization selective beam shaping using nanoscale dielectric metasurfaces. Opt. Express, 2015, 23, 22611-22618.

23 Chong, K. E., Wang, L. Staude, I., James, A.R., Dominguez, J., Liu, S., Subramania, G.S., Decker, M., Neshev, D.N., Brener, I., and Kivshar, Y.S. Efficient Polarization-Insensitive Complex Wavefront Control Using Huygens' Metasurfaces Based on Dielectric Resonant Meta-atoms. ACS Photonics, 2016, 3, 514-519.

24 Zheludev, N. I. Obtaining optical properties on demand. Science, 2015, 348, 973-974.

25 Chen, H.-T., Padilla, W.J., Zide, J.M.O., Gossard, A.C., Taylor, A.J., and Averitt, R.D. Active terahertz metamaterial devices. Nature, 2006, 444, 597-600.

26 Park, J., Kang, J.-H., Liu, X. & Brongersma, M. L. Electrically Tunable Epsilon-Near-Zero (ENZ) Metafilm Absorbers. Sci. Rep., 2015, 5.

27 Wang, Q., Rogers, E.T.F., Gholipour, B., Wang, C.-M., Yuan, G., Teng, J., and Zheludev, N.I. Optically reconfigurable metasurfaces and photonic devices based on phase change materials. Nat. Photonics, 2016, 10, 60-65.

28 Hosseini, P., Wright, C. D. & Bhaskaran, H. An optoelectronic framework enabled by low-dimensional phase-change films. Nature, 2014, 511, 206-211.

29 Shportko, K., Kremers, S., Woda, M., Lencer, D., Robertson, J., and Wuttig, M. Resonant bonding in crystalline phase-change materials. Nat. Mater. , 2008, 7, 653-658.

30 Zheludev, N. I. and Plum, E. Reconfigurable nanomechanical photonic metamaterials. Nat. Nanotechnol., 2016, 11, 16-22.

31 Guo, P., Schaller, R. D., Ketterson, J. B. and Chang, R. P. Ultrafast switching of tunable infrared plasmons in indium tin oxide nanorod arrays with large absolute amplitude. Nat. Photonics, 2016.

32 Wurtz, G. A., Pollard, R., Hendren, W., Wiederrecht, G.P., Gosztola, D.J., Podolskiy, V.A., and Zayata, A.V. Designed ultrafast optical nonlinearity in a plasmonic nanorod metamaterial enhanced by nonlocality. Nat. Nanotechnol., 2011, 6, 107-111.

33 Lewi, T., Evans, H. A., Butakov, N. A. and Schuller, J. A. Ultrawide Thermo-optic Tuning of PbTe Meta-Atoms. Nano Lett., 2017, 17, 3940-3945, doi:10.1021/acs.nanolett.7b01529.

34 Lee, S. H., Choi, M., Kim, T.-T., Lee, S., Liu, M., Yin, X., Choi, H.K., Lee, S.S., Choic, C.-G., Choi, S.-Y., Zhang, X., and Min, B. Switching terahertz waves with gate-controlled active graphene metamaterials. Nat. Mater. , 2012, 11, 936-941.

35 Driscoll, T., Kim, H.-T., Chae, B.-G., Kim, B.-J., Lee, Y.-W., Jokerst, N.M, Palit, S., Smith, D.R., Ventra, M.D., and Basov, D.N. Memory metamaterials. Science, 2009, 325, 1518-1521.

36 Kats, M. A., Sharma, D., L. J., Genevet, P. Blanchard, R., Yang, Z., Qazilbash, M.M, Basov, D.N., Ramanathan, S., and Capasso, F. Ultra-thin perfect absorber employing a tunable phase change material. Appl. Phys. Lett., 2012, 101, 221101.

37 Dicken, M. J., Aydin, K. Pryce, I.M., Sweatlock, L.A., Boyd, E.M., Walavalkar, S., Ma, J., and Atwater, H.A. Frequency tunable near-infrared metamaterials based on VO2 phase transition. Opt. Express, 2009, 17, 18330-18339.

38 Jeong, Y.-G., Bernien, H., Kyoung, J.-S., Park, H.-R., Kim, H.-S., Choi, J.-W., Kim, B.-J., Kim., H.-T, Ahn, K.J., and Kim, D.-S.. Electrical control of terahertz nano antennas on VO2 thin film. Op. Express, 2011, 19, 21211-21215.

39 Kim, M., Jeong, J., Poon, J. K. & Eleftheriades, G. V. Vanadium-dioxide-assisted digital optical metasurfaces for dynamic wavefront engineering. J. Opt. Soc. Am. B, 2016, 33, 980-988.

40 Kaplan, G., Aydin, K. & Scheuer, J. Dynamically controlled plasmonic nano-antenna phased array utilizing vanadium dioxide. Opt. Mater. Express, 2015, 5, 2513-2524.

41 Zimmer, J., Wixforth, A., Karl, H. & Krenner, H. J. Ion beam synthesis of nanothermochromic diffraction gratings with giant switching contrast at telecom wavelengths. Appl. Phys. Lett., 2012, 100, 231911.

42 Appavoo, K., Lei, D.J., Sonnefraud, Y., Wang, B., Pantelides, S.T., Maier, S.A., and Haglund, R.F. Role of defects in the phase transition of VO2 nanoparticles probed by plasmon resonance spectroscopy. Nano Lett., 2012, 12, 780-786.

43 Rini, M. et al. Photoinduced phase transition in VO2 nanocrystals: ultrafast control of surface-plasmon resonance. Opt. Let., 2005, 30, 558-560.

44 Jostmeier, T., Zimmer, J., Karl, H., Krenner, H. J. & Betz, M. Optically imprinted reconfigurable photonic elements in a VO2 nanocomposite. Appl. Phys. Lett., 2014, 105, 071107.

45 Basov, D. N., Averitt, R. D., Van Der Marel, D., Dressel, M. & Haule, K. Electrodynamics of correlated electron materials. Rev. Mod. Phys., 2011, 83, 471.

46 Mun, B. S.Chen, K., Yoon, J., Dejoie, C., Tamura, N., Kunz, M., Liu, Z., Grass, M.E., Mo, S.-K., Park, C., Lee, Y.Y., and Ju, H. Nonpercolative metal-insulator transition in VO2 single crystals. Phys. Rev. B, 2011, 84, 113109.

47 Liu, M.Sternbach, A.J., Wagner, M., Slusar, T.V., Kong, T., Bud'ko, S.L., Kittiwatanakul, S., Qazilbash, M.M., McLeod, A., Fei, Z., Abreu, E., Zhang, J., Goldflam, M., Dai, S., Ni, G.-Z., Lu, J., Bechtel, H.A., Martin, M.C., Raschke, M.B., Averitt, R.D., Wolf, S.A., Kim, H.-T., Canfield, P.C., and Basov, D.N. Phase transition in bulk single crystals and thin films of VO2 by nanoscale infrared spectroscopy and imaging. Phys. Rev. B, 2015, 91, 245155.

48 Qazilbash, M. M., Brehm, M., Chae, B.-G., Ho., P.-C., Andreev, G.O., K., B.-J., Yun, S.J., Balatsky, A.V., Maple, M.B., Keilmann, F., Kim, H.-T., and Basov, D.N. Mott transition in VO2 revealed by infrared spectroscopy and nano-imaging. Science, 2007, 318, 1750-1753.

49 Engheta, N. Circuits with light at nanoscales: optical nanocircuits inspired by metamaterials. Science, 2007, 317, 1698-1702.

50 Lee, D., Lee., J., Song, K., Xue, F., Choi, S.-Y., Ma, Y., Podkaminer, J., Liu, D., Liu, S.-C., Chung, B., Fan, W., Cho, S.J., Zhou, W., Lee, J., Chen, L.-Q., Oh, S.H., Ma, Z., and Eom, C.-B.. Sharpend VO2 Phase Transition via Controlled Release of Epitaxial Strain. Nan. Lett., 2017.

51 Griffiths, C. and Eastwood, H. Influence of stoichiometry on the metal□semiconductor transition in vanadium dioxide. J. Appl. Phys., 1974, 45, 2201-2206.

52 Cao, L., White, J.S., Park, J.-S., Schuller, J.A., Clemens, B.M., and Brongersma, M.L. Engineering light absorption in semiconductor nanowire devices. Nat. Mater. , 2009, 8, 643-647.

533 Schuller, J. A., Zia, R., Taubner, T. & Brongersma, M. L. Dielectric metamaterials based on electric and magnetic resonances of silicon carbide particles. Phys. Rev. Lett., 2007, 99, 107401.

54 Iyer, P., Pendharkar, M., Palmstrøm, C. J. & Schuller, J. A. Ultrawide thermal free-carrier tuning of dielectric antennas coupled to epsilon-near-zero substrates.Nat. Comm., 2017, 8, 472.

55 Cao, L., Fan., P., Vasudev, A.P., White, J.S., Yu, Z. Cai, W., Schuller, J.A., Fan, S., and Brongersma, M.L. Semiconductor nanowire optical antenna solar absorbers. Nano Lett., 2010, 10, 439-445.

56 Atwater, H. A. and Polman, A. Plasmonics for improved photovoltaic devices. Nat. Mater. , 2010, 9, 205-213.

57 Cao, L., Park, J.-S., Fan, P., Clemens, B. and Brongersma, M. L. Resonant germanium nanoantenna photodetectors. Nano Lett., 2010, 10, 1229-1233.

58 Cao, L., Fan, P., Barnard, E. S., Brown, A. M. & Brongersma, M. L. Tuning the color of silicon nanostructures. Nano Lett., 2010, 10, 2649-2654.

59 Butakov, N. and Schuller, J. Hybrid optical antennas with photonic resistors. Opt. Express, 2015, 23, 29698-29707.

60 Lopez, R., Feldman, L. C. and Haglund Jr, R. F. Size-Dependent Optical Properties of VO2 Nanoparticle Arrays. Phys. Rev. Lett., 2004, 93, 177403.

61 Cao, J., Ertekin, E., Srinivasan, Fan, W., Huang, S., Zheng, H., Yim, J.W.L., Khanai, D.R., Ogletree, D.F., Grossman, J.C., and Wu, J. Strain engineering and one-dimensional organization of metal–insulator domains in single-crystal vanadium dioxide beams. Nature Nanotechnol., 2009, 4, 732-737.

61 Fan, W., Cao, J., Seidel, J., Gu, Y., Yim, J.W., Barret, C., Yu, K.M., Ji, J., Ramesh, R., Chen, L.Q., and Wu, J. Large kinetic asymmetry in the metal-insulator transition nucleated at localized and extended defects. Phys. Rev. B, 2011, 83, 235102.

62 Aetukuri, N.B., Gray, A.X., Drouard, M., Cossale, M., Gao, L., Reid, A.H., Kukreja, R., Ohidag, H., Jenkins, C.A., Arenholz, E., Roche, K.P., Durr, H.A., Samant, M.G., and Parkin, S.S.P. Control of the metal-insulator transition in vanadium dioxide by modifying orbital occupancy. Nat. Phys., 2013, 9, 661-666.

63 Iyer, P. P., Pendharkar, M. and Schuller, J. A. Electrically reconfigurable metasurfaces using heterojunction resonators. Adv. Opt. Mater., 2016.

64 Joushaghani, A., Jeong, J., Paradis, S., Alain, D., Aitchison, J.S., Poon, J.K.S. Wavelength-size hybrid Si-VO2 waveguide electroabsorption optical switches and photodetectors. Opt. Express, 2015, 23, 3657-3668.

65 Iyer, P. P., Butakov, N. A. and Schuller, J. A. Reconfigurable semiconductor phased-array metasurfaces. ACS Photonics 2015, 2, 1077-1084.

66 Lewi, T., Iyer, P. P., Butakov, N. A., Mikhailovsky, A. A. and Schuller, J.A. Widely tunable infrared antennas using free carrier refraction. Nano Lett., 2015, 15, 8188-8193.

67 Fischer, M.P., Schmidt, C., Sakat, E., Stock, J., Samarelli, A., Frigerio, J., Ortolani, M., Paul, D.J., Isella, G., Leitenstorfer, A., Biagioni, P., and Brida, D. Optical Activation of Germanium PlasmonicNanoantennas in the Mid Infrared. arXiv preprint arXiv:1603.06339 (2016).

68 Baranov, D. G., Makarov, S.V., Milichko, V.A., Kudryashov, S.I., Krasnok, A.E., and Belov, P.A. Nonlinear Transient Dynamics of Photoexcited Resonant Silicon Nanostructures. ACS Photonics, 2016.

69 Shcherbakov, M. R., Vabishchevich, A.S., Chong, K.E., Choi, D.-Y., Staude, I., Miroshnichenko, A.E., Neshev, D.N., Fedyanin, A.A., and Kivshar, Y.S. Ultrafast all-optical switching with magnetic resonances in nonlinear dielectric nanostructures. Nano Lett., 2015, 15, 6985-6990.

70 McLeod, A. van Heumen, E., Ramirez, J.G., Wang, S., Saerbech, T., Guenon, S., Goldflam, M., Andreregg, L., Kelly, P., Mueller, A., Liu, M.K., Schuller, I.K., and Basov, D.N. Nanotextured phase coexistence in the correlated insulator V2O3. Nat. Phys., 2016.

71 Stewart, M., Brownstead, D., Wang, S., West, K.G., Ramirez, J.G., Qazilbash, M.M., Perkins, N.B., Schuller, I.K., and Basov, D.N. Insulator-to-metal transition and correlated metallic state of V2O3 investigated by optical spectroscopy. Phys. Rev. B, 2012, 85, 205113.

72 Li, Z., Zhou, Y., Qi, H., Pan, Q., Zhang, Z., Shi, N.N., Lu, M., Stein, A., Li, C.Y., Ramanathan, S., and Yu, N. Correlated Perovskites as a New Platform for Super-Broadband-Tunable Photonics. Adv. Mater., 2016, 28, 9117-9125.

73 Mikheev, E., Hauser, A.J., Himmetoglu, B., Moreno, N.E., Janotti, A., Van de Walle, C.G., and Stemmer, S.. Tuning bad metal and non-Fermi liquid behavior in a Mott material: Rare-earth nickelate thin films. Sci. Adv., 2015, 1, e1500797.

Funding

This work was supported by the Air Force Office of Scientific Research (FA9550-16-1-0393 and FA9550-12-1-0381) and by the UC Office of the President Multi-campus Research Programs and Initiatives (MR-15-328528). Numerical calculations for this work were performed on the computing cluster at the Center for Scientific Computing from the California NanoSystems Institute at the University of California, Santa Barbara: an NSF MRSEC (DMR-1121053) and NSF CNS-0960316. We acknowledge support from the Vannevar Bush Faculty Fellowship program sponsored by the Basic Research Office of the Assistant Secretary of Defense for Research and Engineering and funded by the Office of Naval Research through grant N00014-15-1-2848. Thin films were prepared at the UCSD Nanoscience Center and nanostructures were fabricated at the UCSB Nanofabrication Facility. This research was conducted with government support under the DoD, Air Force Office of Scientific Research, National Defense Science and Engineering Graduate (NDSEG) Fellowship, 32 CFR 168a.

Acknowledgements

This is highly collaborative research. J.A.S. and N.A.B. conceived the ideas for the research project. I.V. and C.U. grew the thin films, characterized them and performed transport measurements. Z.R. and S.W. grew the single-crystal samples. T.L. and A.A.M fabricated the VO_2 spheres. N.A.B. performed the numerical simulations, sample fabrication, and optical characterization. N.A.B. and J.A.S. wrote the original draft of the manuscript, which then underwent multiple iterations between all the coauthors. J.A.S and I.K.S. supervised the research project. We thank Kirk Post and Dmitri Basov for their assistance in temperature-dependent ellipsometry measurements. We are grateful for discussions with Prasad Iyer, Tomer Lewi, Tanya Das, and Steven Brown.

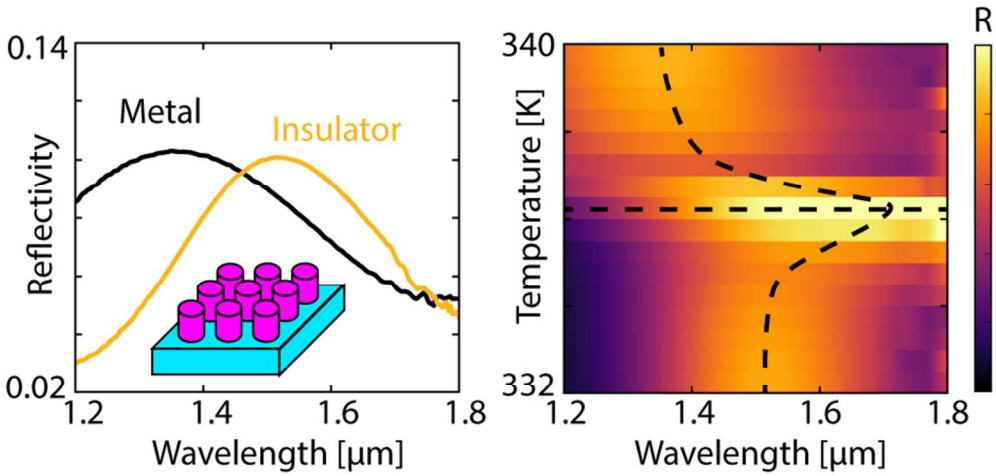

Table of Contents Figure

80x40mm (300 x 300 DPI)

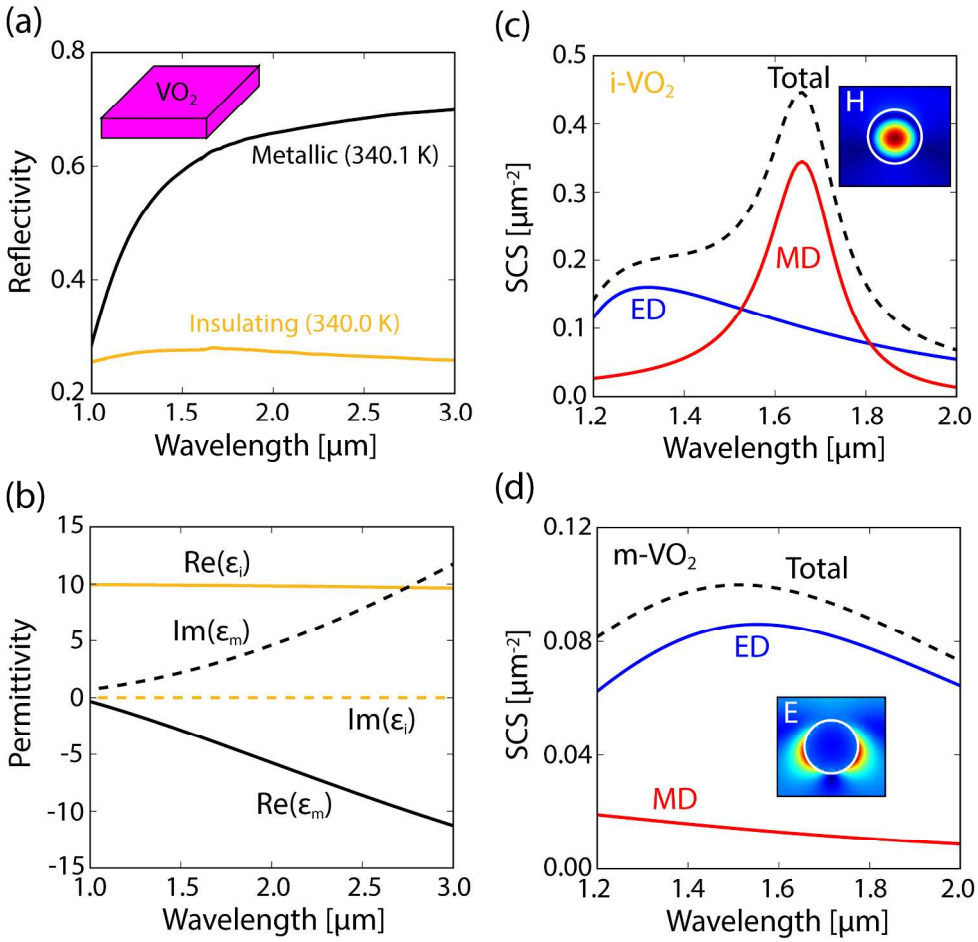

Reflectivity of VO2 Single Crystals. (a) Near-infrared reflectivity of a VO2 single crystal in its low-temperature insulating phase (orange curve) and high-temperature metallic phase (black curve). (b) Real (solid curve) and imaginary (dashed curve) components of the fitted VO2 optical permittivity in the insulating phase (orange curve) and metallic phase (black curve). Scattering-cross-section of a (c) insulating, and (d) metallic VO2 sphere in air, with diameter d=500 nm, calculated with Mie theory. Insets corresponds to simulated local (c) magnetic, and (d) electric, field profile at the fundamental resonance. Crystal growth, optical characterization, Mie Theory calculation, and simulation details are included in the Supporting Information.

226x213mm (300 x 300 DPI)

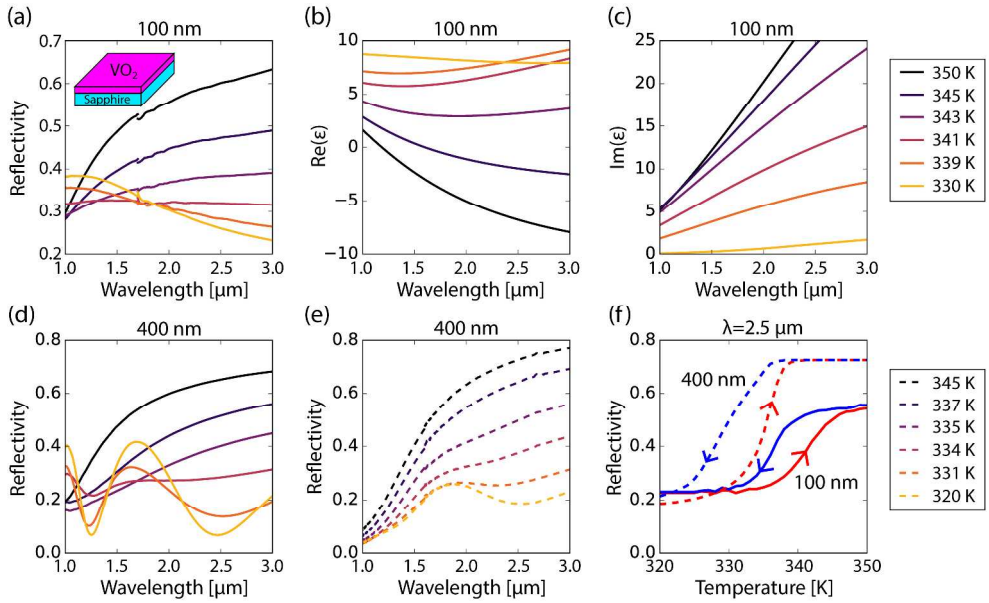

VO2 Thin-Film Reflectivity and Optical Constants (a) The measured FTIR reflectivity of a 100 nm VO2 film on a sapphire substrate. The (b) real, and (c) imaginary components of the optical permittivity, as determined by a spectral fit to the measured reflectivity. Experimental and fitting details are provided in the Methods and Supplementary Material. (d) The simulated reflectivity of a 400 nm thick VO2 film, based on the 100 nm optical constants. (e) The measured reflectivity of a 400 nm thick VO2 film. (f) The optical hysteresis of the 100 nm film (solid line) and 400 nm film (dashed line) at a wavelength λ=2.5 μm. Sample fabrication, measurement details, and mid-infrared spectra are included in the Supporting Information.

340x206mm (300 x 300 DPI)

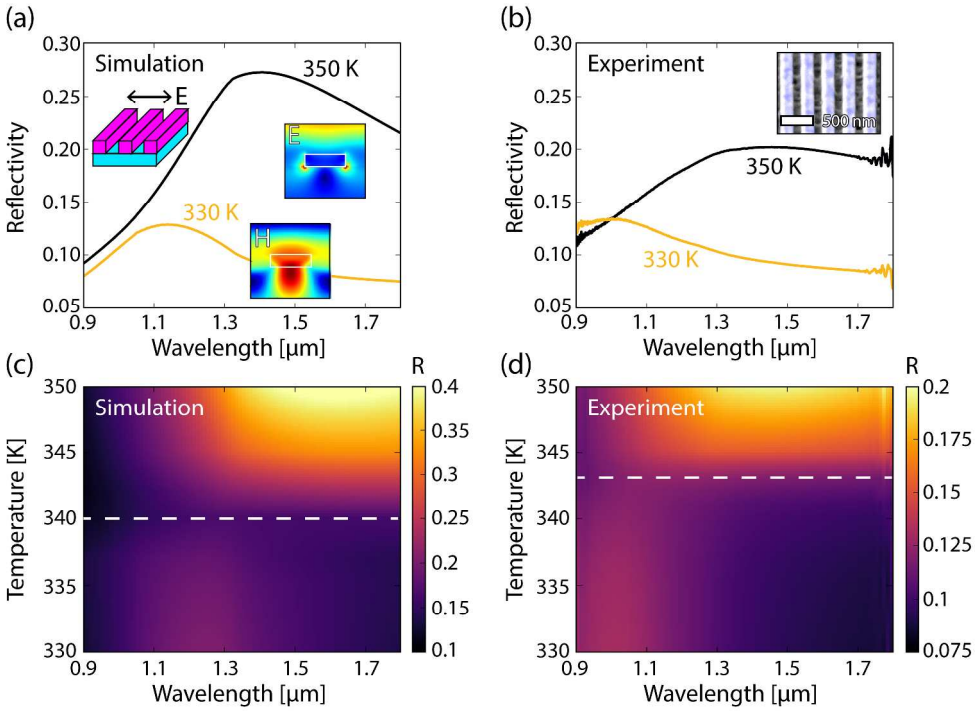

TE-Polarized VO2 Wire Array Reflectivity. (a) Simulated reflectivity of a VO2 wire array, on sapphire, in the insulating and metallic phases, under TE-polarized illumination based on optical constants found for a 100 nm VO2 film. Insets corresponding to the magnetic-field profiles at the insulating resonance, and electric-field profiles at the metallic resonance. (b) Experimentally measured reflectivity of the corresponding VO2 wire array, in the insulating and metallic phases. Inset is an SEM of the fabricated structure. (c) Simulated, and (d) experimentally measured, reflectivity of the array, including intermediate temperatures. Note that the color scale in (d) is different relative to (c) to increase clarity. Wires are rectangular with width w=280 nm, height h=100 nm, and pitch a=500 nm. Simulation and experimental details are included in the Supporting Information.

289x207mm (300 x 300 DPI)

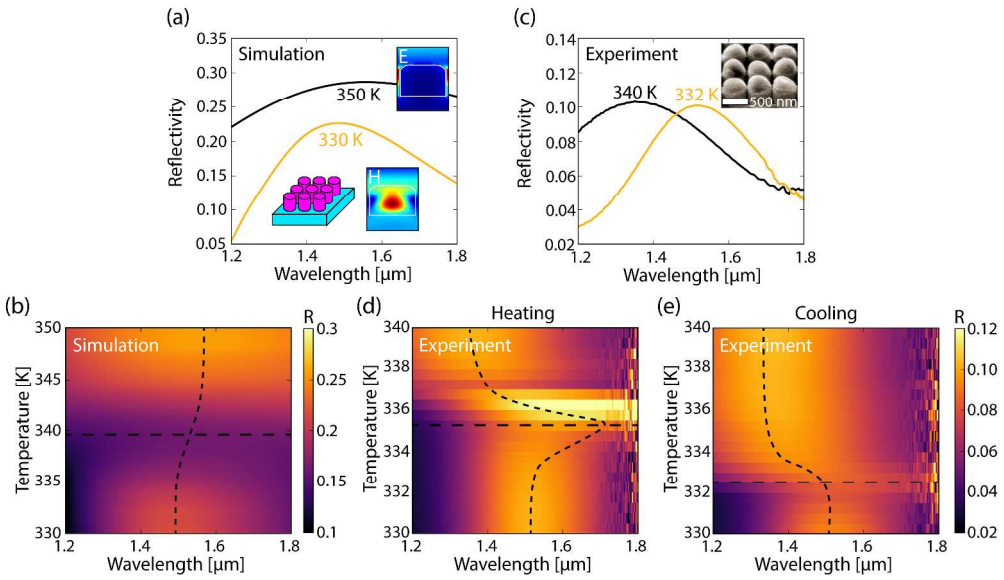

Figure 4 –VO2 Disk Array Reflectivity. (a) Simulated reflectivity of a VO2 disk array. Disk resonators have a height h=500 nm, diameter d=480 nm, and pitch a=500 nm based on optical constants from a 100 nm film. Insets correspond to local field distributions at the resonant peaks. (b) Simulated reflection as a function of temperature and wavelength. Vertical dashed curve tracks the reflectivity peak, horizontal dashed line represents the transition temperature (c) Experimentally measured reflectivity of VO2 disk array (with approximate height h=400 nm, diameter d=480 nm, and pitch a=500) above and below transition. Inset is an SEM of the fabricated structure. (d) Experimental reflection data, upon heating, including intermediate temperatures. (e) Experimental reflection data, upon cooling, including intermediate temperatures. Vertical dashed curve tracks the reflectivity peak, horizontal dashed line represents the transition temperature. Note that the temperature span in (d,e) is different than (c). Simulation and experimental details are included in the Supporting Information.

366x209mm (300 x 300 DPI)